Red, green, and blue simultaneous generation in aperiodically poled Zn-diffused $LiNbO_3:Er^{3+}/Yb^{3+}$ nonlinear channel waveguides

E. Cantelar,[a] G. A. Torchia, J. A. Sanz-García, P. L. Pernas, G. Lifante, and F. Cussó
Departamento de Física de Materiales, C-IV, Universidad Autónoma de Madrid, 28049 Madrid, Spain

(Received 31 March 2003; accepted 13 August 2003)

In this work, continuous-wave broadly tunable simultaneous generation of red (650–690 nm), green (520–575 nm), and blue (425–495 nm) light in aperiodically poled Zn-diffused $LiNbO_3:Er^{3+}/Yb^{3+}$ channel waveguides is reported after Ti:sapphire excitation in the 850–990 nm range. The red and green emissions arise from energy transfer and upconversion mechanisms between Yb^{3+} and Er^{3+} ions, while the blue light with a maximum efficiency of 0.04% $W^{-1}\,cm^{-1}$ is produced by quasi-phase matching processes. © *2003 American Institute of Physics.*
[DOI: 10.1063/1.1617367]

Lithium niobate ($LiNbO_3$) compares favorably with other ferroelectric crystals for nonlinear optical applications not only because of its large nonlinear coefficients but also because of the possibility of modulating them, offering the option of nonlinear frequency conversion via quasi-phase matching (QPM) processes. Several nonlinear devices based on periodic (PPLN) or aperiodically (APPLN) poled $LiNbO_3$ have been reported, including the additional advantage of using waveguiding structures, where high power densities are easily available.[1–8]

In this work, nonlinear channel waveguides fabricated by Zn diffusion in Er^{3+}/Yb^{3+} codoped APPLN are used to generate simultaneous red, green, and blue (RGB) light. APPLN crystals were grown by the off-centered Czochralski method, along the *a* axis, with automatic diameter control by a crucible-weighting technique. The initial melts containing congruent $LiNbO_3$ ($[Li]/[Nb]=0.945$) were doped with Er_2O_3 and Yb_2O_3 with a purity grade of 99.99%.

The growth conditions, pulling and rotation rates and the seed crystal shift, were adjusted appropriately to favor the formation of modulated ferroelectric domain distributions[9] in order to achieve red, green, and blue light under excitation in the 880–1040 nm spectral range (Yb^{3+} absorption band). Using this procedure chirped-period-poled domain structures are obtained. The domain pattern from a *y*-cut wafer was revealed by etching in a diluted solution of $HF:HNO_3$ (1:2 by volume) for 1 h and then checked by conventional optical microscopy. As illustrated in Fig. 1, the wafer exhibits several chirped-period-poled domain structures with periods ranging from 5 to 16 μm, being the averaged period of $\sim 7\,\mu$m.

The wafer was then polished to optical grade in order to fabricate the channel waveguides by Zn diffusion.[7,10,11] In the present work, the metal diffusion was performed following a two-step procedure (exchange and diffusion)[12–14] which preserves the initial wafer ferroelectric pattern.[15] The exchange process at 550 °C for 2 h was performed followed by annealing in open atmosphere at 850 °C for 4 h. These conditions produce a 4 μm depth Gaussian index profile, with a maximum index change of 0.15% and 0.20% in the extraordinary and ordinary refractive indices, respectively. These waveguides support two modes in the visible range and are single mode at the IR pump wavelengths used in the experiments.

The experimental configuration used in the measurements, crystal axis and polarization of the incident and output beams, has also been sketched in Fig. 1. The beam from a Ti:sapphire laser operating at 920 nm was end-coupled into a 4 μm width and 1 cm length channel waveguide as TE propagating mode. The IR beam can excite the Yb^{3+} ions or it can interact with the d_{33} nonlinear coefficient of $LiNbO_3$. As a consequence, a strong white spot is appreciated when the output from the waveguide is focused on a screen. If the output from the waveguide is dispersed with a prism, four intense spots were spatially separated and distinguished with the naked eye (Fig. 2). From right to left, blue, green, and red colors are clearly observed, besides an additional spot originated from the IR pump beam, which appears as ''white'' due to saturation effect of the imaging device.

In order to ascertain the origin of these three colors, the waveguide output was directed to the entrance slit of a monochromator and the dispersed light was detected with a photomultiplier tube. Figure 3 shows the emission spectrum measured in a 4 μm width channel waveguide in the visible range (450–700 nm). As can be seen, the output light is the combination of two broad emission bands in the red and in the green regions of the spectra, and a narrow line in the blue region.

The blue emission (right spot in Fig. 2) is due to SHG of the 920 nm pump light in the channel waveguide. Blue emission is produced only when the IR beam, ω wave, is coupled as the extraordinary wave (TE propagating mode). The polarization of the blue light, 2ω wave, is the same as that of

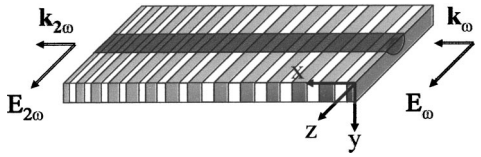

FIG. 1. Experimental configuration used in the measurements.

[a]Electronic mail: eugenio.cantelar@uam.es

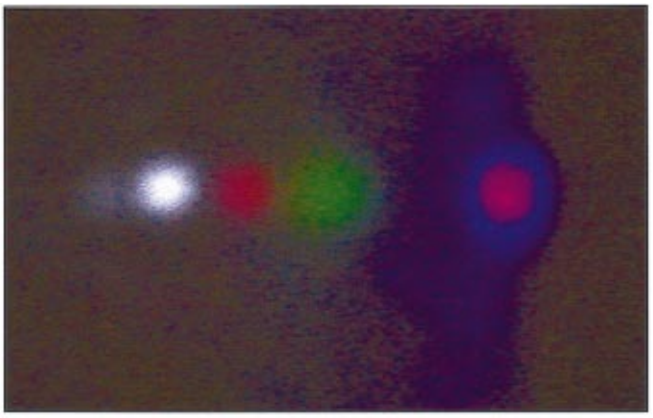

FIG. 2. (Color) Image of the output waveguide focused on a screen, after being spatially separated with a prism.

the ω wave as indicated in Fig. 1. The SH intensity shows a quadratic dependence on the ω-wave intensity, as expected for a second-order frequency conversion process.

The maximum efficiency observed was 0.04% $W^{-1}\,cm^{-1}$ for fundamental wavelengths around 970 nm (2ω wave around 485 nm). The chirped-period-poled domain structures provide a large set of reciprocal vectors for quasi-phase matching compensation (QPM) at expense of peak efficiency,[4,16] as a consequence the SH signal exhibits a broadly tunable band. This point is illustrated in Fig. 4, which shows a series of blue light emissions obtained for a discrete set of fundamental excitation wavelengths.

The red and green emission bands, after IR excitation, are due to energy transfer upconversion processes (ETU) involving Er^{3+} and Yb^{3+} ions, following the mechanisms sketched in Fig. 5. The pump, 880–1040 nm spectral range, excites the Yb^{3+} ions to the $^2F_{5/2}$ manifold from where they relax by radiative and nonradiative transitions or by different energy transfer mechanisms involving Er^{3+} ions.[17] After Yb^{3+} absorption, the excitation can be transferred to the $^4I_{11/2}$ Er^{3+} level, via the cross relaxation mechanism $^2F_{5/2} \rightarrow {}^2F_{7/2}:{}^4I_{15/2} \rightarrow {}^4I_{11/2}$. Additionally, a second cross relaxation from Yb^{3+} to a previously excited Er^{3+} ion leads to the excitation of the Er^{3+} ion to the upper levels via the ETU process $^2F_{5/2} \rightarrow {}^2F_{7/2}:{}^4I_{11/2} \rightarrow {}^4F_{7/2}$. The $^4F_{7/2}$ Er^{3+} level relaxes nonradiatively to the $^2H_{11/2}:{}^4S_{3/2}$ manifolds from where the radiative decay to the ground state generates the green emission band and the nonradiative connection populates the red luminescent level, $^4F_{9/2}$. On the other hand, the $^4I_{13/2}$ Er^{3+} level can also accept the energy transfer from Yb^{3+} ions.[18] In this case, the $^4F_{9/2}$ Er^{3+} level receives an extra contribution to its population via the ETU process $^2F_{5/2} \rightarrow {}^2F_{7/2}:{}^4I_{13/2} \rightarrow {}^4F_{9/2}$. The inset in Fig. 3 illustrates how this extra contribution, measured in codoped samples with fixed Er^{3+} concentration (0.7% mol) and variable Yb^{3+} concentration, increases the red to green intensity ratio by increasing the Yb^{3+} concentration.

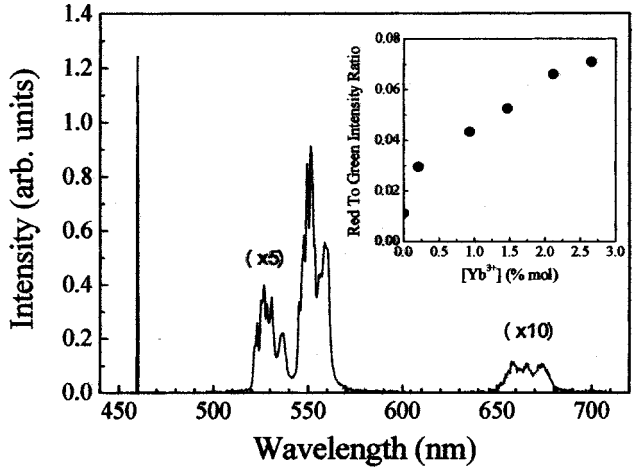

FIG. 3. Emission spectrum after pumping at 920 nm. Inset shows the ratio between red and green emissions measured in samples with fixed Er^{3+} concentration (0.7% mol) and variable Yb^{3+} concentrations.

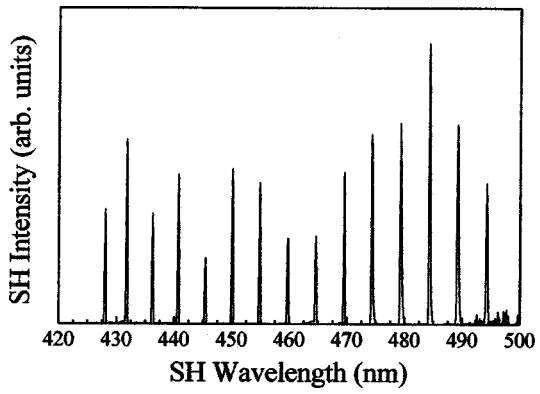

FIG. 4. SH signal measured in the channel waveguide corresponding to a discrete set of fundamental wavelengths between 850 and 990 nm.

The dependencies on pump power of both emissions were found to be lower than the expected quadratic law for a two photon process. This fact could be related with the presence of saturation effects or due to the presence of several competing population paths: energy transfer from Yb^{3+} ions and absorption of the blue light within the Er^{3+} ions ($^4I_{15/2} \rightarrow {}^4F_{5/2,3/2}$ absorption band).

In conclusion, stable, simultaneous continuous-wave RGB generation in Zn-diffused Er^{3+}/Yb^{3+} codoped APPLN channel waveguides has been obtained at RT. The red (650–690 nm) and green (520–575 nm) colors are produced by ETU processes between the Er^{3+} and Yb^{3+} ions, while the blue signal is due to SHG involving the d_{33} nonlinear coefficient of $LiNbO_3$. Although with a limited efficiency in the

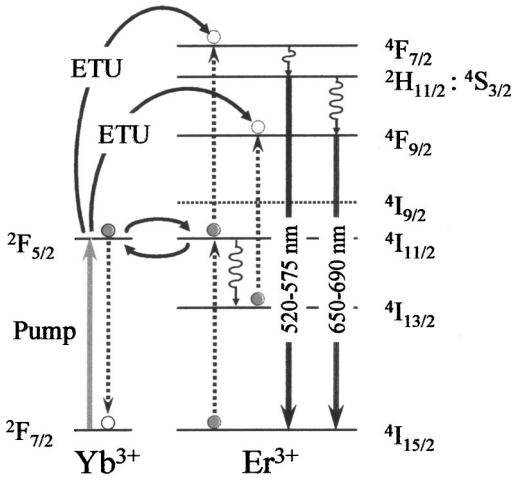

FIG. 5. Energy level diagram of Er^{3+} and Yb^{3+} ions showing the energy transfer processes between both ions.

blue generation (0.04% $W^{-1}\,cm^{-1}$), it has been proved that Zn-diffused $LiNbO_3:Er^{3+}/Yb^{3+}$ nonlinear channel waveguides can be used for RGB generation with broad tunability (880–1060 nm).

This work was partially supported under Project Nos. TIC2001-0226 and TIC2002-00147. G.A.T. is supported by a grant from MECD (Spain).

[1] M. M. Fejer, G. A. Magel, D. H. Jundt, and R. L. Byer, IEEE J. Quantum Electron. **28**, 2631 (1992).
[2] M. Houé and P. D. Townsend, J. Phys. D **28**, 1747 (1995).
[3] V. Pruneri, S. Butterworth, and D. C. Hanna, Appl. Phys. Lett. **69**, 1029 (1996).
[4] J. Capmany, D. Callejo, V. Bermúdez, E. Diéguez, D. Artigas, and L. Torner, Appl. Phys. Lett. **79**, 293 (2001).
[5] C. W. Hsu and C. C. Yang, Opt. Lett. **26**, 1412 (2001).
[6] D. J. L. Birkin, E. U. Rafailov, G. S. Sokolovskii, W. Sibbett, G. W. Ross, P. G. R. Smith, and D. C. Hanna, Appl. Phys. Lett. **78**, 3172 (2001).
[7] M. Fujimura, A. Shiratsuki, T. Suhara, and H. Nishihara, Jpn. J. Appl. Phys., Part 2 **37**, L659 (1998).
[8] H. Suche, G. Schreiber, Y. L. Lee, V. Quiring, R. Ricken, W. Sohler, A. Paoletti, F. Carbone, D. Caccioli, and A. Schiffini, Proceedings of the European Conference Optic Communications (ECOC'01), **6**, 42 (2001).
[9] E. P. Kokanyan, V. G. Babajanyan, and G. G. Demirkhanyan, J. Appl. Phys. **92**, 1544 (2002).
[10] W. M. Young, R. S. Feigelson, M. M. Tejer, M. J. F. Digonnet, and H. J. Shaw, Opt. Lett. **16**, 995 (1991).
[11] W. M. Young, M. M. Fejer, M. J. F. Digonnet, A. F. Marshall, and R. S. Feigelson, J. Lightwave Technol. **10**, 1238 (1992).
[12] R. Nevado and G. Lifante, Appl. Phys. A: Mater. Sci. Process. **72**, 725 (2001).
[13] P. L. Pernas, M. J. Hernández, E. Ruíz, E. Cantelar, R. Nevado, C. Morant, G. Lifante, and F. Cussó, Appl. Surf. Sci. **161**, 123 (2000).
[14] R. E. Di Paolo, E. Cantelar, P. L. Pernas, G. Lifante, and F. Cussó, Appl. Phys. Lett. **79**, 4088 (2001).
[15] R. Nevado, E. Cantelar, G. Lifante, and F. Cussó, Jpn. J. Appl. Phys., Part 2 **39**, L488 (2000).
[16] H. Liu, S. N. Zhu, Y. Y. Zhu, N. B. Ming, X. C. Lin, W. J. Ling, A. Y. Yao, and Z. Y. Xu, Appl. Phys. Lett. **81**, 3326 (2002).
[17] E. Cantelar, J. A. Muñoz, J. A. Sanz-García, and F. Cussó, J. Phys.: Condens. Matter **10**, 8893 (1998).
[18] E. Cantelar and F. Cussó, J. Lumin. **102-103**, 525 (2003).